Title
The histone H3-H4 tetramer is a copper reductase enzyme

Journal
Science, 369(6499)

ISSN
0036-8075

Authors
Attar, Narsis
Campos, Oscar A
Vogelauer, Maria
et al.

Publication Date
2020-07-03

DOI
10.1126/science.aba8740

Peer reviewed

HHS Public Access

Author manuscript

Science. Author manuscript; available in PMC 2021 January 28.

Published in final edited form as:

Science. 2020 July 03; 369(6499): 59–64. doi:10.1126/science.aba8740.

The Histone H3-H4 Tetramer is a Copper Reductase Enzyme

Narsis Attar[1,2,†], **Oscar A. Campos**[1,2,†], **Maria Vogelauer**[1,†], **Chen Cheng**[1], **Yong Xue**[1], **Stefan Schmollinger**[3,#], **Lukasz Salwinski**[1,3], **Nathan V. Mallipeddi**[1], **Brandon A. Boone**[1], **Linda Yen**[4], **Sichen Yang**[1], **Shannon Zikovich**[1], **Jade Dardine**[1], **Michael F. Carey**[1,2], **Sabeeha S. Merchant**[3,#], **Siavash K. Kurdistani**[1,2,5,*]

[1]Department of Biological Chemistry, David Geffen School of Medicine, University of California Los Angeles, Los Angeles, CA 90095, USA

[2]Molecular Biology Institute, University of California Los Angeles, Los Angeles, CA 90095, USA

[3]UCLA-DOE Institute, University of California Los Angeles, Los Angeles, CA 90095, USA

[4]Department of Molecular, Cell, and Developmental Biology, University of California Los Angeles, Los Angeles, CA 90095, USA

[5]Eli and Edythe Broad Center of Regenerative Medicine and Stem Cell Research, David Geffen School of Medicine, University of California Los Angeles, Los Angeles, CA 90095, USA

Abstract

The eukaryotic histone H3-H4 tetramer contains a putative Cu^{2+} binding site at the interface of the apposing H3 proteins with unknown function. The coincident emergence of eukaryotes with global oxygenation, which challenged cellular copper utilization, raised the possibility that histones may function in cellular copper homeostasis. We report that the recombinant Xenopus H3-H4 tetramer is an oxidoreductase enzyme that binds Cu^{2+} and catalyzes its reduction to Cu^{1+} *in vitro*. Loss- and gain-of-function mutations of the putative active site residues correspondingly altered copper binding and the enzymatic activity, as well as intracellular Cu^{1+} levels and copper-dependent mitochondrial respiration and Sod1 function in the yeast *S. cerevisiae*. The histone H3-H4 tetramer, therefore, constitutes a novel mechanism for generation of biousable Cu^{1+} ions in eukaryotes.

One Sentence Summary: The histone H3-H4 tetramer catalyzes cupric ion reduction to support cellular copper utilization.

*Correspondence to: skurdistani@mednet.ucla.edu.

#Current address: QB3-Berkeley, University of California Berkeley, Berkeley, CA 94720, USA

†These authors contributed equally, and are listed alphabetically

Author contributions: Conceptualization, N.A., O.A.C., M.V., Y.X., and S.K.K.; Methodology, N.A., O.A.C., M.V., Y.X., M.F.C., S.S.M., and S.K.K.; Investigation, N.A., O.A.C., M.V., Y.X., C.C., S.S., L.S., N.M., B.A.B., L.Y., S.Y., S.Z., J.D., and S.K.K.; Formal Analysis, N.A., O.A.C., and M.V.; Writing – Original Draft, N.A., O.A.C., M.V., and S.K.K.; Writing – Review & Editing, N.A., O.A.C., M.V., Y.X., L.Y., S.S., M.F.C., S.S.M. and S.K.K.; Resources, N.A., O.A.C., M.V., C.C., L.Y., M.F.C., S.S.M., and S.K.K.; Visualization, N.A., O.A.C., and M.V.; Supervision, S.K.K.; Project Administration, S.K.K.; Funding Acquisition, M.F.C., S.S.M., and S.K.K.

Competing interests: The authors declare no competing interests.

Data and materials availability: All data are available in the main text or the supplementary materials. Gene expression datasets are available on the NCBI GEO database (GSE100034).

Eukaryotes owe their nucleosomal chromatin structure to ancestral histone-containing archaea. Archaeal histones form a structure similar to the eukaryotic H3-H4 tetramer (1) but unlike eukaryotic histones, typically lack extended N-terminal tails and post-translational modifications. Archaea also have smaller genomes than eukaryotes, and no nuclei. The little apparent capability for epigenetic regulation or need for genome compaction in archaea prompted us to consider whether the conserved histone H3-H4 tetramer may have an additional function.

An overlooked feature of the nucleosome and the geochemical events surrounding eukaryogenesis hinted at what such a function might be. The dimerization interface of the two histone H3 proteins contains cysteine and histidine residues (Fig. 1A) in an arrangement typical of Cu^{2+} binding sites in other proteins (2). The evolutionary conservation of residues in this region is greater than expected from their contributions to nucleosome stability (3), consistent with a potential metal binding capability (4–6).

The emergence of eukaryotes coincided approximately with the initial accumulation of oxygen (7), which decreased the biousability and increased the toxicity of transition metals such as copper (8). The hypothesis that histones may have facilitated metal utilization in oxidizing conditions has not been considered.

Copper often serves as a redox co-factor for enzymes such as cytochrome *c* oxidase in the mitochondrial electron transport chain (ETC) and Cu, Zn-superoxide dismutases (e.g., Sod1) (9). As a redox co-factor, copper cycles between the cupric (Cu^{2+}) and cuprous (Cu^{1+}) states. However, it is the cuprous form that is trafficked and sensed intracellularly, suggesting a need to maintain cellular copper in the Cu^{1+} oxidation state for proper distribution and utilization (10). Whether protein-based mechanisms have evolved to regulate intracellular Cu^{2+} reduction is unknown. Here, we present evidence that the eukaryotic H3-H4 tetramer binds Cu^{2+}, catalyzes Cu^{2+} reduction and improves the utilization of copper by nuclear, cytoplasmic and mitochondrial proteins.

Recombinant histone H3-H4 tetramer binds cupric ions

To determine whether copper ions interact with the residues at the H3-H3’ interface (4) (Fig. 1A–B), we assembled and purified recombinant *Xenopus laevis* wildtype (Xl WT) histone H3-H4 tetramers (11) (fig. S1A–C). Incubation of the Xl WT tetramer with increasing amounts of Cu^{2+} in a Tricine buffer resulted in a UV absorbance band that is characteristic of copper-cysteine interactions (12) (Fig. 1C, fig. S1D). UV absorbance plateaued at a molar ratio of ~1, suggesting a stoichiometry of one copper ion per tetramer (Fig. 1C, fig. S1D). Mutation of C110 to alanine (*H3C110A*) (fig. S1B–C) abolished this copper-dependent absorbance change (Fig. 1C). Isothermal Titration Calorimetry (ITC) analysis further demonstrated high affinity of the tetramer for Cu^{2+} and an approximately equimolar stoichiometry (Fig. 1D). The WT H3-H4 complex also exhibited greater retention on a Cu^{2+} affinity column than the $H3^{C110A}$ counterpart (fig. S1E).

The histone H3-H4 tetramer catalyzes cupric ion reduction

We next hypothesized that a mechanism to maintain the Cu^{1+} state intracellularly may be beneficial in oxidizing conditions. Thus, we asked whether the H3-H4 tetramer catalyzes the reduction of Cu^{2+} to Cu^{1+} in the presence of a source of electrons. We developed an assay utilizing chelators neocuproine (NC) or bicinchoninic acid (BCA) to detect Cu^{1+} production spectrophotometrically (fig. S2A, Fig. 2A). Assays contained reduced forms of either tris(2-carboxyethyl)phosphine (TCEP), nicotinamide adenine dinucleotide (NADH), or its phosphate form (NADPH), as electron donors. Reactions were initiated by addition of Cu^{2+} in the form of either $CuCl_2$-Tricine, $CuCl_2$-N-(2-Acetamido)iminodiacetic acid (ADA), or $CuCl_2$-Nitrilotriacetic acid (NTA) solutions (fig. S2B). Spontaneous Cu^{1+} production occurred at a slow rate, but the rate of Cu^{1+} production substantially increased in the presence of the Xl WT tetramer (Fig. 2B, fig. S2C–E). Production of Cu^{1+} eventually plateaued due to near full consumption of the electron source (Fig. 2B). No significant production of Cu^{1+} occurred in the absence of TCEP, indicating that it, and not the tetramer, was the source of electrons. The tetramer enhanced Cu^{2+} reduction in anaerobic conditions as well, ruling out any role for oxygen (fig. S2F). The Xl WT tetramer assembled into a complex with the C-terminus of the human histone chaperone Spt2 (13) also enhanced Cu^{2+} reduction (fig. S2G–I). Additionally, the tetramer could utilize natural reductants such as NADPH to increase Cu^{2+} reduction (fig. S3A). Direct measurement of NADPH confirmed its oxidation during Cu^{2+} reduction (fig. S3B). The effect of the tetramer was specific to cupric ions as there was no enhancement of ferric ion reduction.

Heating (Fig. 2B) or Proteinase K digestion (fig. S3C) of the Xl WT tetramer abolished Cu^{2+} reduction activity. The unassembled Xl histone H3 or the yeast H2A also did not enhance Cu^{2+} reduction (fig. S3C–D). Increasing rates of Cu^{1+} production occurred with increasing amounts of either TCEP (Fig. 2C) or Cu^{2+} (Fig. 2D), eventually approaching a maximum rate, consistent with protein-based catalysis (fig. S3E–F).

The *H3C110A* mutation substantially reduced the rate of Cu^{2+} reduction (Fig. 2E), as did treatment with *N*-ethylmaleimide (NEM) (fig. S3G). RNase A, which contains redox reactive cysteines (14), did not enhance Cu^{2+} reduction (fig. S3H). Similarly, DTT directly reduced an equimolar amount of Cu^{2+} but did not substantially enhance the rate of Cu^{2+} reduction by TCEP (fig. S3H). These data underscore the importance of H3C110 to the tetramer enzyme activity.

Mutation of H3H113 (4, 5) to alanine (*H3H113A*), or to asparagine or tyrosine (*H3H113N* or *H3H113Y*) which have been found in certain cancers (15), had little effect on the rate of reduction with Cu^{2+}-Tricine as the substrate but diminished Cu^{2+} reduction with Cu^{2+}-ADA (Fig. 2F, fig. S2B) or Cu^{2+}-NTA as substrates (fig. S2B, fig. S3I), likely due to the differing Cu^{2+} coordination ability of different buffers. Altogether, our data reveal that the H3-H4 tetramer catalyzes Cu^{2+} reduction by various electron donors and is thus a cupric reductase.

The yeast histone H3 contains H113 but lacks the C110 residue found in most other eukaryotic H3s (Fig. 1B). Consistently, recombinant yH3-H4 tetramer did not absorb UV light in the 245 nm range when incubated with Cu^{2+}. However, a broad peak centered at 680

nm was observed at high concentrations of yeast tetramer and high ionic strength (2 M NaCl), consistent with weakly-absorbing d-d transitions typical of coordinated Cu^{2+} ions (16) (Fig. 3A, fig. S4A). The *H3H113A* mutation (fig. S4B–C) decreased the copper-dependent absorbance change at 680 nm (Fig. 3A). Furthermore, retention of the yH3-H4 complex on a Cu^{2+} affinity column was reduced by the *H3H113A, N,* or *Y* mutations (fig. S4B–F), consistent with a role of H3H113 in Cu^{2+} interaction.

Mutation of H3A110 to cysteine ($yH3^{A110C}$ tetramer) (fig. S4G–H) elicited a copper-dependent UV absorbance band nearly identical to that observed with the Xl WT tetramer (Fig. 3B). Furthermore, the *H3H113A* mutation of the $yH3^{A110C}$ tetramer (i.e. $yH3^{A110CH113A}$ tetramer) (fig. S4G–I) diminished copper-dependent absorbance at 245 nm (Fig. 3B), indicating that H3H113 affects the cysteine-Cu^{2+} interaction. The $yH3^{A110C}$ tetramer also displayed cupric reductase activity, which was diminished by the *H3H113A* mutation (Fig. 3C). In the absence of H3C110, the yeast tetramer did not display cupric reductase activity in standard salinity, likely due to deficient Cu^{2+} binding, which required 2 M NaCl (Fig. 3A). High salinity interfered with other assay components, precluding further investigation. Nonetheless, our findings suggest that the yH3-H4 tetramer can display cupric reductase activity, and that H3H113 participates in this function.

Mutation of histone H3H113 results in loss of function in yeast

We next investigated whether mutation of the H3H113 residue *in vivo* would diminish the Cu^{1+} pool. Mutation of H3H113 to alanine is lethal in *S. cerevisiae* (17) (fig. S5A). However, introduction of either *H3H113N* or *H3H113Y* mutations in the two chromosomal copies of the histone H3 gene generated viable and somewhat slow growing yeast strains $H3^{H113N}$ and $H3^{H113Y}$ (fig. S5B). Yeast strains in which the *H3H113N* and *H3H113Y* mutant histones were expressed from one locus, with the other locus deleted, were severely sick compared to strains expressing both histone loci (fig. S5C). This finding identifies *H3H113N* and *H3H113Y* as loss-of-function alleles, coincident with the loss of Cu^{2+} binding *in vitro*. We mostly utilized the *H3H113N* mutation in genetic experiments because *H3H113Y* results in a more severe growth defect, potentially confounding the interpretation of phenotypes.

H3H113 mutations alter cuprous ion availability

We next assayed the activity of the transcription factor Mac1 as a readout of nuclear Cu^{1+} abundance because it is directly inhibited by Cu^{1+} and does not bind Cu^{2+} (18). Gene expression analysis revealed largely similar profiles in WT and $H3^{H113N}$ strains in rich fermentative media (SC and YPD) (fig. S6A). However, Mac1 target genes were upregulated in both the $H3^{H113N}$ (fig. S6B) and $H3^{H113Y}$ strains (Fig. 4A). Deletion of *CTR1*, the main copper importer in yeast (19), expectedly increased Mac1 target expression (Fig. 4B, fig. S6B–C). However, Mac1 targets displayed even greater upregulation and incomplete repression in response to exogenous copper in $H3^{H113N}ctr1\Delta$ (Fig. 4B, fig. S6C). Importantly, *ctr1*Δ substantially reduced total copper levels whereas the *H3H113N* mutation did not (Fig. 4C), suggesting that the H3H113 mutations decrease Cu^{1+} levels without affecting total copper abundance.

We developed a reporter plasmid to assess Cu^{1+} abundance by employing the Cup2 transcription factor, which is directly activated by Cu^{1+} but not Cu^{2+} (20). The plasmid harbors the *GFP* gene downstream of the *CUP1* promoter, which is the main target of Cup2 (21) (Fig. 4D, fig. S6D). GFP expression was proportional to the expected Cu^{1+} levels in both physiological and genetic assays (Fig. 4E, fig. S6E–F), and was reduced in $H3^{H113N}$ (Fig. 4F, fig. S6G), further indicating that H3H113 is required to maintain cellular Cu^{1+} levels.

The H3H113 residue supports copper utilization for mitochondrial respiration

We next asked whether the H3H113 mutations impair copper utilization outside the nucleus. We first tested mitochondrial respiration via copper-dependent cytochrome *c* oxidase function. Although $H3^{H113N}$ did not display a defect in mitochondrial respiration, the $H3^{H113Y}$ strain displayed a significant loss of O_2 consumption (Fig. 5A, fig. S7A). This defect was exacerbated in presence of the copper chelator bathocuproinedisulfonic acid (BCS) and was recovered by excess exogenous copper (fig. S7B–C).

To relate the defects in mitochondrial respiration to disruption of copper utilization, we assessed the ability of cells to increase respiratory function as they were shifted from a copper-depleted state to a copper-replete state. Copper depletion via *CTR1* deletion resulted in a low rate of antimycin-sensitive O_2 consumption (Fig. 5B, fig. S7D) and cytochrome *c* oxidase activity (Fig. 5C), which were gradually increased by addition of exogenous copper. However, substantially more copper was required to rescue *ctr1*Δ in the context of *H3H113N* (Fig. 5B–C). More copper was also required to rescue respiratory growth of *ctr1*Δ in the context of *H3H113N* or *H3H113Y* (Fig. 5D, fig. S7E). *H3H113N* also diminished the copper-dependent rescue of cells lacking *MAC1*, which activates *CTR1* expression (18) (fig. S7F). Addition of iron, zinc, or manganese did not rescue the respiratory growth defects of *ctr1*Δ strains (fig. S7G).

Consistent with the hypomorphic nature of *H3H113N*, a strain with one WT H3 and one *H3H113N* gene displayed an intermediate defect compared to strains containing two *H3H113N* or two WT H3 genes (fig. S8A). Similarly, deleting one of the two copies of the H3 and H4 genes (*hht1-hhf1*Δ) (fig. S8B–D) increased the copper requirement in *ctr1*Δ for respiratory growth (fig. S8E).

Total copper and iron levels were similar between $H3^{H113N}$ and WT in respiratory medium (Fig. 5E, fig. S9A). Addition of excess copper increased total copper levels similarly in both strains (Fig. 5E), indicating that the copper utilization defect in $H3^{H113N}$*ctr1*Δ was not due to changes in total copper abundance. Inefficient recovery of *ctr1*Δ in the context of *H3H113N* was not due to increased Cu^{1+} sequestration by the metallothionein Cup1 because loss of Cup1 ($cup1^{F8stop}$) had no effect on the requirement for copper in $H3^{H113N}$*ctr1*Δ (fig. S9B).

We considered whether potential disruptions in chromatin accessibility or gene regulation account for the copper utilization defects of the H3H113 mutants. The *H3H113N* mutation

or deletion of Asf1, a histone chaperone that facilitates nucleosome assembly in part through interaction with H3H113 (22, 23), resulted in minimal disruption of chromatin accessbility (fig. S9C). However, *asf1*Δ did not phenocopy the H3H113 mutants in respiratory media (fig. S9D). Global gene expression patterns were similar between WT and $H3^{H113N}$ strains in respiratory media (fig. S9E), with comparable upregulation of genes involved in respiratory growth and copper regulation (fig. S9F–G).

Deletion of membrane-bound metalloreductases *FRE1* and *FRE2* (24) did not phenocopy the H3H113 mutations (fig. S10A), suggesting that the intracellular role of histone H3 on copper utilization is distinct from extracellular metal reduction. Glutathione (GSH) also participates in cellular copper metabolism (25). Decreasing GSH levels, by deleting the *GSH1* gene, increased the amount of copper required to rescue *ctr1*Δ but to a lesser extent than *H3H113N* (fig. S10B). Importantly, combining *H3H113N* with *gsh1*Δ caused an even greater defect in copper utilization (fig. S10B), suggesting that histones have a unique role in copper utilization.

Histone H3 supports copper utilization for Sod1 function.

We next considered whether histone H3 might also affect copper utilization by Sod1. Total Sod1 activity was ~40% less in $H3^{H113Y}$ compared to WT, which was recovered by excess exogenous copper (fig. S11A–B). *H3H113N* also decreased Sod1 activity by ~20% (Fig. 5F). Deletion of *CTR1* reduced Sod1 activity and formation of its internal disulfide bond, which are dependent on Cu^{1+} and the copper chaperone Ccs1 (26) (Fig. 5F). Combining *ctr1*Δ with *H3H113N* further decreased the internal disulfide bond and Sod1 activity, which were restored by addition of excess exogenous copper (Fig. 5F). Loss of function of Sod1 causes lysine auxotrophy in yeast (27). Correspondingly, $H3^{H113N}$*ctr1*Δ exhibited a growth defect in lysine deficient conditions (fig. S11C).

Deletion of *CCS1* significantly decreased Sod1 activity (Fig. 5G), which was restored by addition of excess copper, but the *H3H113N* mutation substantially increased the amount of copper required for recovery (Fig. 5G). Considerably more copper was also required to rescue the lysine auxotrophy of *ccs1*Δ in the context of *H3H113N* (fig. S11D–E). Unlike the effect of *H3H113N*, deletion of *CTR1* did not increase the requirement of *ccs1*Δ for exogenous copper (fig. S11F), suggesting that histones contribute to copper utilization differently than Ctr1. Excess copper did not rescue the lysine auxotrophy of *sod1*Δ strains (fig. S11G), whereas hypoxia rescued the lysine auxotrophy of *ccs1*Δ and *sod1*Δ regardless of H3H113 (fig. S11H), indicating that the H3H113 is relevant to this phenotype when Sod1 function is required.

Addition of manganese, zinc, or iron did not rescue *ccs1*Δ lysine auxotrophy (fig. S11I). The increased copper requirement of $H3^{H113N}$*ccs1*Δ was not due to differences in Cup1-dependent Cu^{1+} sequestration (fig. S12A), intracellular copper and iron levels (fig. S12B–C) or Asf1 (fig. S11E). Gene expression differences also did not account for defective copper utilization as *ccs1*Δ and $H3^{H113N}$*ccs1*Δ displayed similar patterns (fig. S12D–F). Altogether, our findings reveal that the H3H113 residue is also important for copper utilization by Sod1.

The significant impacts of H3H113 mutations on Cu^{1+} abundance and on at least three separate copper-dependent functions support the model that the cupric reductase function of the H3-H4 tetramer regulates Cu^{1+} availability in yeast.

The *H3A110C* mutation enhances cuprous ion availability and copper utilization.

The *in vitro* copper reductase results suggested that *H3A110C* might serve as a gain-of-function mutation to increase Cu^{1+} and improve copper utilization *in vivo*. The yeast $H3^{A110C}$ strain grew similarly to WT cells (fig. S13A) but enhanced the ability of exogenous copper to restore the respiratory growth of *ctr1*Δ (Fig. 6A). We reasoned that increased provision of Cu^{1+} might mitigate the depletion of cellular GSH. Indeed, $H3^{A110C}$*gsh1*Δ grew better than *gsh1*Δ in copper-depleted respiratory conditions (fig. S13B) with a greater O_2 consumption rate (Fig. 6B, fig. S13C). $H3^{A110C}$ exhibited a copper-dependent growth advantage in the presence of a sub-lethal amount of potassium cyanide, an inhibitor of cytochrome *c* oxidase, independently of GSH levels (Fig. 6C, fig. S13D). Correspondingly, the $H3^{A110C}$*gsh1*Δ strain displayed greater Cup2 activity than *gsh1*Δ (Fig. 6D), indicating increased Cu^{1+} abundance. Additionally, the *H3A110C* mutation enhanced the copper-dependent rescue of lysine auxotrophy in *ccs1*Δ (Fig. 6E). The *H3A110C* mutation even rescued the diminished Cup2 activity of $H3^{H113N}$ (fig. S13E), the copper utilization defect of the $H3^{H113N}$*ctr1*Δ strain (Fig. 6F), and remarkably, the lethality of the *H3H113A* mutation (Fig. 6G), corroborating the opposing effects of the H3A110 and H3H113 mutations both *in vivo* and *in vitro*. These results highlight the advantage in copper utilization conferred by the *H3A110C* mutation and further support that the yeast histone H3 regulates the Cu^{1+} pool and copper utilization.

Discussion

Histones have been known as packaging and regulatory proteins for the eukaryotic genome. We now reveal that the histone H3-H4 tetramer is also a cupric reductase that provides biousable Cu^{1+} for the cell. The enzymatic activity suggests the protein complex has many uncharacterized features, including a catalytic site at the H3-H3' interface, that contribute to Cu^{2+} binding, increasing its reduction potential and promoting electron transfer (28).

The H3-H3' interface forms *in vivo* mostly during nucleosome assembly. Therefore, the commencement of enzymatic activity may be coupled to the protection of DNA as it wraps around the nucleosome. Such a coupling may decrease the toxicity of Cu^{1+} by the very enzymes that produce it as a beneficial adaptation in species that require its intracellular use. However, proteins such as Spt2 (13), may stabilize the H3-H3' interface outside of the nucleosomal context, affecting regulation and timing of enzymatic activity relative to other chromatin-based events.

The mechanism of electron transfer by the tetramer is unclear but may involve direct transfer from reductants to Cu^{2+} at the active site or through a chain of residues from a distant site (29, 30). Copper is present in the nucleus (31, 32), but is likely bound (33) and transported to and from histones through as-yet-to-be-identified chaperones, possibly including Atox1

(34). Interestingly, copper disproportionately accumulates in the nucleus when its cellular efflux is compromised such as in Wilson's disease (35, 36), suggesting that the nucleus is a major transit hub for cellular copper.

The oxidoreductase function of the H3-H4 tetramer provides a reasonable hypothesis for why the archaeal ancestor of the eukaryotes possessed histone tetramers. Such enzymatic activity, with an associated intracellular Cu^{1+} transit system, could have helped maintain a functioning ETC in the proto-mitochondria, thereby making the presence of histones in the ancestral archaeon not incidental (37), but rather essential for eukaryogenesis.

Supplementary Material

Refer to Web version on PubMed Central for supplementary material.

Acknowledgements

We thank Heather Christofk for discussions, Mayo Thompson for proofreading, Marco Morselli for RNA-seq assistance, Valeria Culotta for the anti-SOD1 antibody and helpful guidance in Sod1 assays, Martin Phillips and William Silkworth of the UCLA-DOE Institute, and the UCLA Broad Stem Cell Center Sequencing Core.

Funding: This work was supported by a W. M. Keck Foundation Award to S.K.K. and S.S.M., and NIH grants CA178415 to S.K.K., GM074701 to M.F.C., GM42143 to S.S.M., and CA188592 to M.V.. O.A.C was supported by the Whitcome; O.A.C. and C.C. by UCLA Dissertation Year Fellowships; N.A. by the NCI Ruth L. Kirschstein NRSA CA186619 and NIH GM8042; L.S. by NIH GM123126; L.Y. by the NCI Ruth L. Kirschstein NRSA GM007185; S.Z. by the Amgen Scholars Program; the UCLA JCCC flow cytometry core by NIH P30 CA016042 and 5P30 AI028697; and the UCLA-DOE Institute by DE-FC02-02ER63421.

References

1. Mattiroli F. et al., Science 357, 609–611 (2017). [PubMed: 28798133]
2. Katz AK et al., Helv Chim Acta 86, 1320–1338 (2003).
3. Ramachandran S, Vogel L, Strahl BD, Dokholyan NV, PLoS computational biology 7, e1001042 (2011).
4. Saavedra RA, Science 234, 1589-1589 (1986). [PubMed: 3787266]
5. Adamczyk M, Poznanski J, Kopera E, Bal W, FEBS Lett 581, 1409–1416 (2007). [PubMed: 17350622]
6. Bal W, Lukszo J, Jezowska-Bojczuk M, Kasprzak KS, Chem Res Toxicol 8, 683–692 (1995). [PubMed: 7548750]
7. Anbar AD, Science 322, 1481–1483 (2008). [PubMed: 19056967]
8. Saito MA, Sigman DM, Morel FMM, Inorg Chim Acta 356, 308–318 (2003).
9. Nevitt T, Ohrvik H, Thiele DJ, Biochim et Biophys Acta 1823, 1580–1593 (2012).
10. Pufahl RA et al., Science 278, 853–856 (1997). [PubMed: 9346482]
11. Dyer PN et al., Method Enzymol 375, 23–44 (2004).
12. Solomon EI, Lowery MD, LaCroix LB, Root DE, Method Enzymol 226, 1–33 (1993).
13. Chen S. et al., Genes Dev 29, 1326–1340 (2015). [PubMed: 26109053]
14. Klink TA, Woycechowsky KJ, Taylor KM, Raines RT, Eur J Biochem 267, 566–572 (2000). [PubMed: 10632727]
15. Forbes SA et al., Nucleic Acids Res 43, D805–D811 (2015). [PubMed: 25355519]
16. Mesu JG et al., Inorg Chem 45, 1960–1971 (2006). [PubMed: 16499357]
17. Huang HL et al., Genome Res 19, 674–681 (2009). [PubMed: 19218532]
18. Graden JA, Winge DR, Proc Nat Acad Sci USA 94, 5550–5555 (1997). [PubMed: 9159110]

19. Dancis A, Haile D, Yuan DS, Klausner RD, J Biol Chem 269, 25660–25667 (1994). [PubMed: 7929270]
20. George GN, Byrd J, Winge DR, J Biol Chem 263, 8199–8203 (1988). [PubMed: 3286647]
21. Thiele DJ, Mol Cell Biol 8, 2745–2752 (1988). [PubMed: 3043194]
22. Agez M. et al., Structure 15, 191–199 (2007). [PubMed: 17292837]
23. Adkins MW, Howar SR, Tyler JK, Mol Cell 14, 657–666 (2004). [PubMed: 15175160]
24. Hassett R, Kosman DJ, J Biol Chem 270, 128–134 (1995). [PubMed: 7814363]
25. Freedman JH, Ciriolo MR, Peisach J, J Biol Chem 264, 5598–5605 (1989). [PubMed: 2564391]
26. Furukawa Y, Torres AS, O'Halloran TV, Embo J 23, 2872–2881 (2004). [PubMed: 15215895]
27. Lin SJ, Culotta VC, Mol Cell Biol 16, 6303–6312 (1996). [PubMed: 8887660]
28. Liu J. et al., Chem Rev 114, 4366–4469 (2014). [PubMed: 24758379]
29. Lucas MF, Rousseau DL, Guallar V, Biochim Biophys Acta 1807, 1305–1313 (2011). [PubMed: 21419097]
30. Williams KR et al., J Am Chem Soc 119, 613–614 (1997).
31. McRae R, Lai B, Fahrni CJ, Metallomics 5, 52–61 (2013). [PubMed: 23212029]
32. Yang LC et al., Proc Nat Acad Sci USA 102, 11179–11184 (2005). [PubMed: 16061820]
33. Rae TD, Schmidt PJ, Pufahl RA, Culotta VC, O'Halloran TV, Science 284, 805–808 (1999). [PubMed: 10221913]
34. Itoh S. et al., J Biol Chem 283, 9157–9167 (2008). [PubMed: 18245776]
35. Huster D. et al., Am J Pathol 168, 423–434 (2006). [PubMed: 16436657]
36. Burkhead JL, Ralle M, Wilmarth P, David L, Lutsenko S, J Mol Biol 406, 44–58 (2011). [PubMed: 21146535]
37. Sandman K, Reeve JN, Science 280, 501, 503 (1998). [PubMed: 9575089]
38. Davey CA, Sargent DF, Luger K, Maeder AW, Richmond TJ, J Mol Biol 319, 1097–1113 (2002). [PubMed: 12079350]
39. Gross C, Kelleher M, Iyer VR, Brown PO, Winge DR, J Biol Chem 275, 32310–32316 (2000). [PubMed: 10922376]
40. Brachmann CB et al., Yeast 14, 115–132 (1998). [PubMed: 9483801]
41. Mann RK, Grunstein M, Embo J 11, 3297–3306 (1992). [PubMed: 1505519]
42. Storici F, Resnick MA, Method Enzymology 409, 329–345 (2006).
43. Ryan OW et al., Elife 3, e03703 (2014).
44. Longtine MS et al., Yeast 14, 953–961 (1998). [PubMed: 9717241]
45. Goldstein AL, McCusker JH, Yeast 15, 1541–1553 (1999). [PubMed: 10514571]
46. Luger K, Mader AW, Richmond RK, Sargent DF, Richmond TJ, Nature 389, 251–260 (1997). [PubMed: 9305837]
47. Luger K, Rechsteiner TJ, Richmond TJ, Method Enzymol 304, 3–19 (1999).
48. Hong L, Bush WD, Hatcher LQ, Simon J, J Phys Chem B 112, 604–611 (2008). [PubMed: 18027923]
49. Rando OJ, Method Enzymol 470, 105–118 (2010).
50. Schmitt ME, Brown TA, Trumpower BL, Nucleic Acids Res 18, 3091–3092 (1990). [PubMed: 2190191]
51. Kim D. et al., Genome Biol 14, R36 (2013). [PubMed: 23618408]
52. Xu G. et al., Source code for biology and medicine 6, 2 (2011). [PubMed: 21232146]
53. Gregg C, Kyryakov P, Titorenko VI, J Vis Exp, 1417 (2009).
54. Spinazzi M, Casarin A, Pertegato V, Salviati L, Angelini C, Nat Protoc 7, 1235–1246 (2012). [PubMed: 22653162]
55. Leitch JM et al., J Biol Chem 284, 21863–21871 (2009). [PubMed: 19542232]
56. Choi B, Rempala GA, Kim JK, Scientific reports 7, 17018 (2017). [PubMed: 29208922]

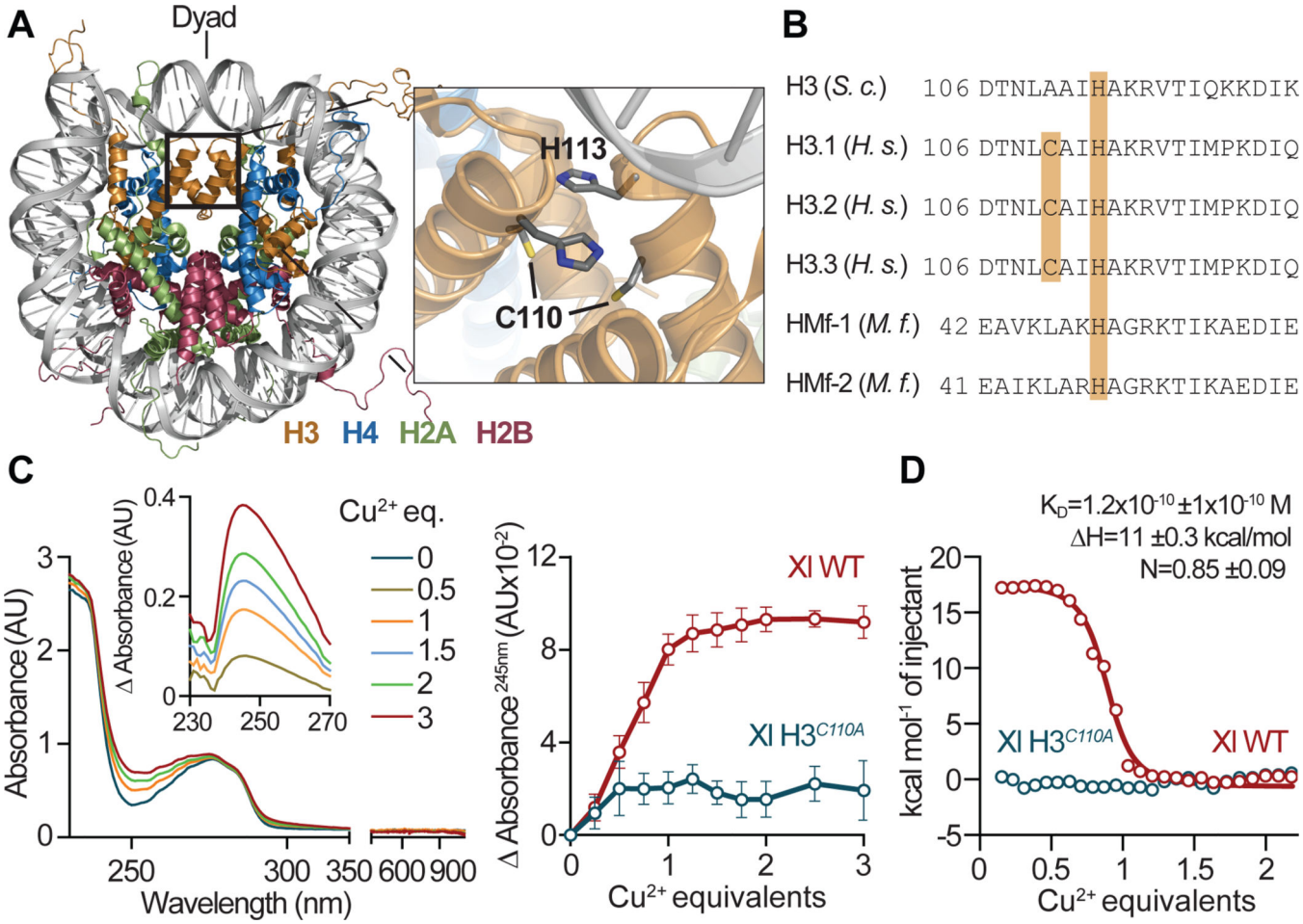

Figure. 1. Recombinant *X. laevis* histone H3-H4 tetramer interacts with cupric ions.

(A) *Left*: *X. laevis* (Xl) nucleosome core particle structure (PDB:1KX5) (38). The box delineates the H3-H3' interface. *Right*: Interface residues H3H113 and H3C110 are shown. **(B)** Alignment of the C-terminal region of *S. cerevisiae* and *H. sapiens* histone H3 and archaeal (*M. fervidus*) histones. **(C)** *Left:* UV-vis absorbance spectrum of the Xl H3-H4 tetramer incubated with or without Cu^{2+}. *Inset*: Differential absorbance compared to tetramer without Cu^{2+}. *Right:* Buffer-corrected differential absorbance of the indicated Xl tetramers. **(D)** Representative ITC titration profile of the Xl H3-H4 tetramer. Circles are experimental data and the line is the fitted curve. Average dissociation constant, enthalpy change, and stoichiometry (N) ±SD of the H3-H4 tetramer-Cu^{2+} complex calculated from three experiments are shown.

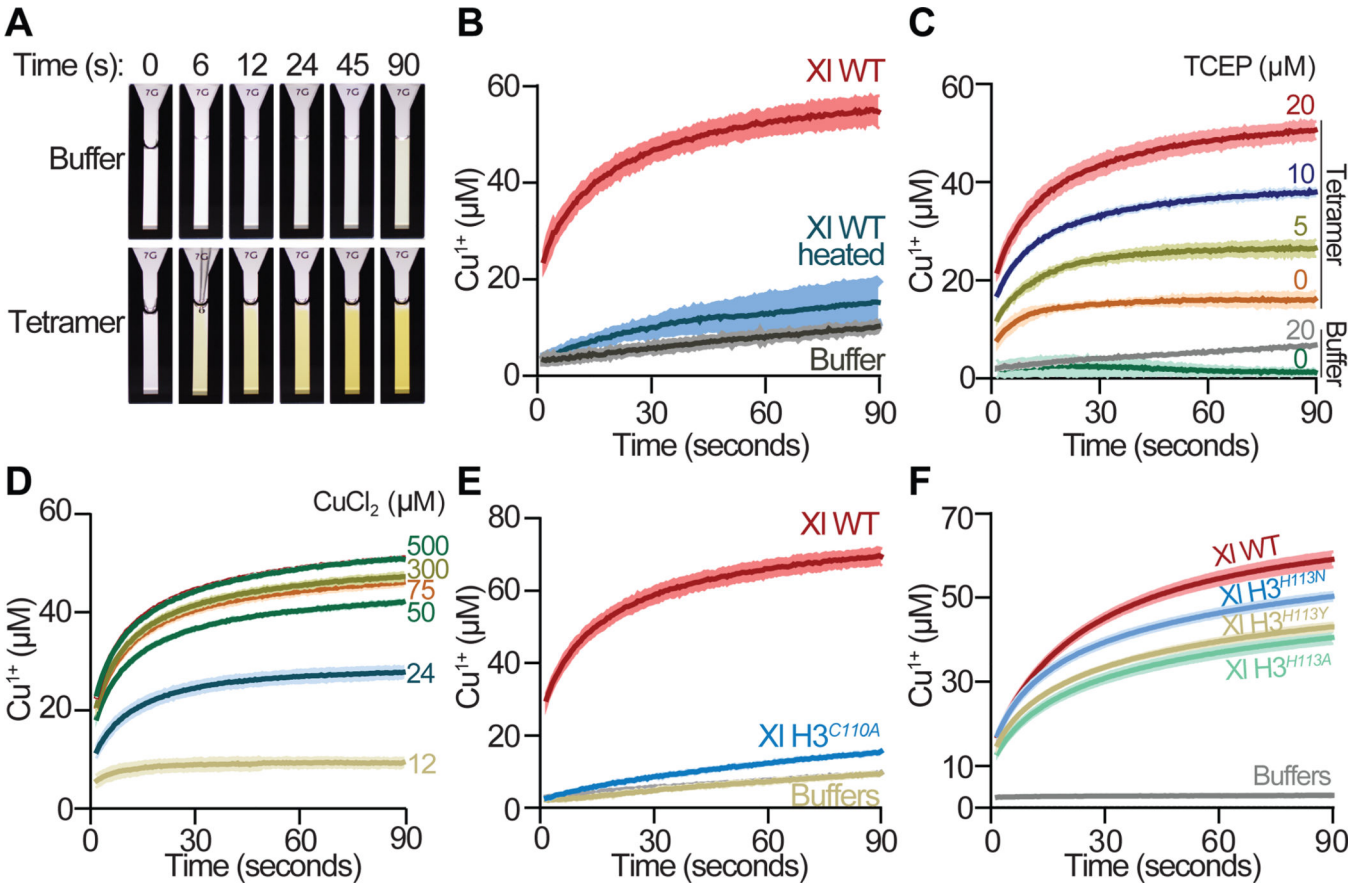

Figure. 2. The *Xenopus laevis* H3-H4 tetramer catalyzes reduction of cupric ions.

(A) Photographic representation of *in vitro* Cu^{2+} reduction assay. The yellow color is due to NC_2-Cu^{1+} complex formation. **(B)** Progress curves of Cu^{2+} reduction with 1 μM of tetramer, heated tetramer, or buffer in presence of 30 μM TCEP and 1 mM $CuCl_2$-10 mM Tricine. Lines and shading represent the mean ±SD of 3–5 assays. **(C-F)** Same as (B) but with the indicated amount of **(C)** TCEP or **(D)** $CuCl_2$; or with **(F)** 5 μM of tetramers in presence of 100 μM TCEP and 0.5 mM $CuCl_2$-ADA pH 8.

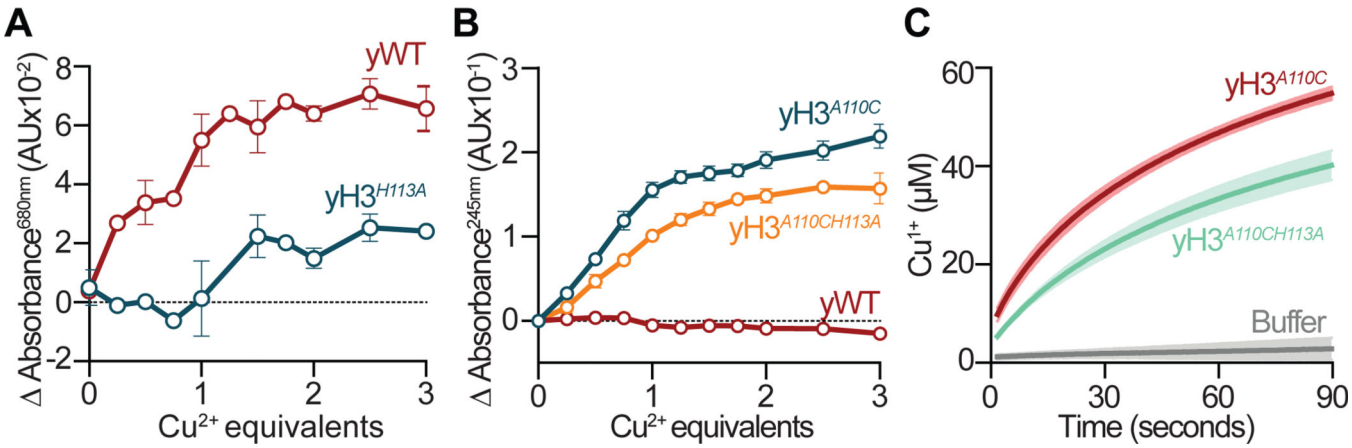

Figure. 3. The yeast H3-H4 tetramer potentially is a copper reductase.

(A-B) Buffer-corrected differential absorbance of the indicated yeast tetramers. **(C)** Progress curves of Cu^{2+} reduction with 5 μM of tetramers in presence of 100 μM TCEP and 0.5 mM $CuCl_2$-ADA pH 8.

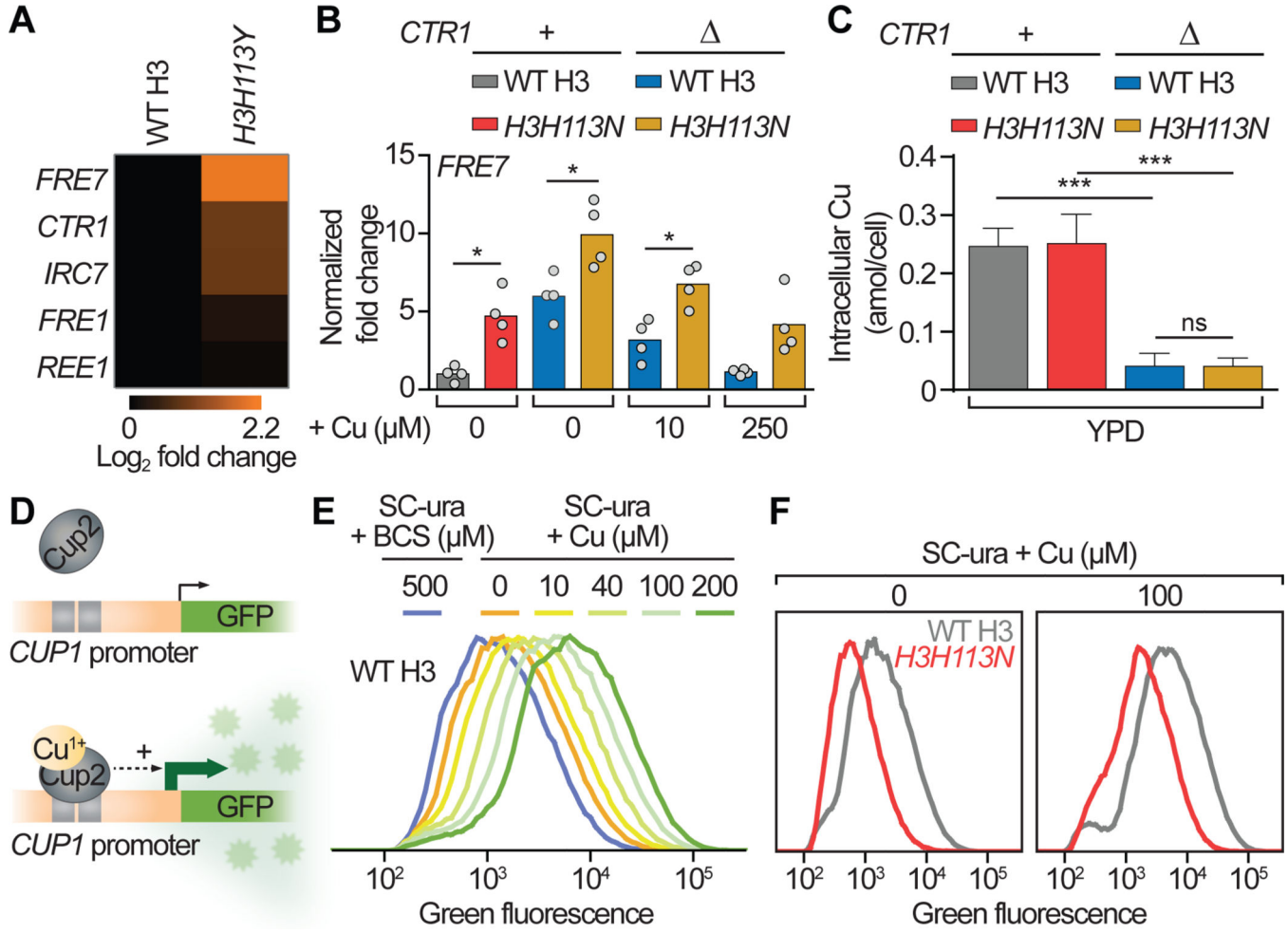

Figure. 4. H3H113 regulates Cu^{1+}-dependent transcriptional activities of Mac1 and Cup2.

(A-B) RT-qPCR analyses of Mac1 target gene (39) expression relative to WT and normalized to *ACT1* expression. Boxes **(A)** and bars **(B)** show means from four independent experiments (dots) in YPD ±$CuSO_4$. Baseline copper concentration in YPD is ~1 μM. **(C)** Intracellular copper content of exponentially growing strains. Bars are means ±SD from 3–6 experiments. **(D)** Schematic representation of the $p^{(CUP1)}$-GFP reporter system. **(E-F)** Average flow cytometry distributions of cells containing the $p^{(CUP1)}$-GFP plasmid grown in SC-ura ±BCS or $CuSO_4$ from 5–6 experiments. Baseline copper concentration in SC is ~0.25 μM. ***P≤0.001.

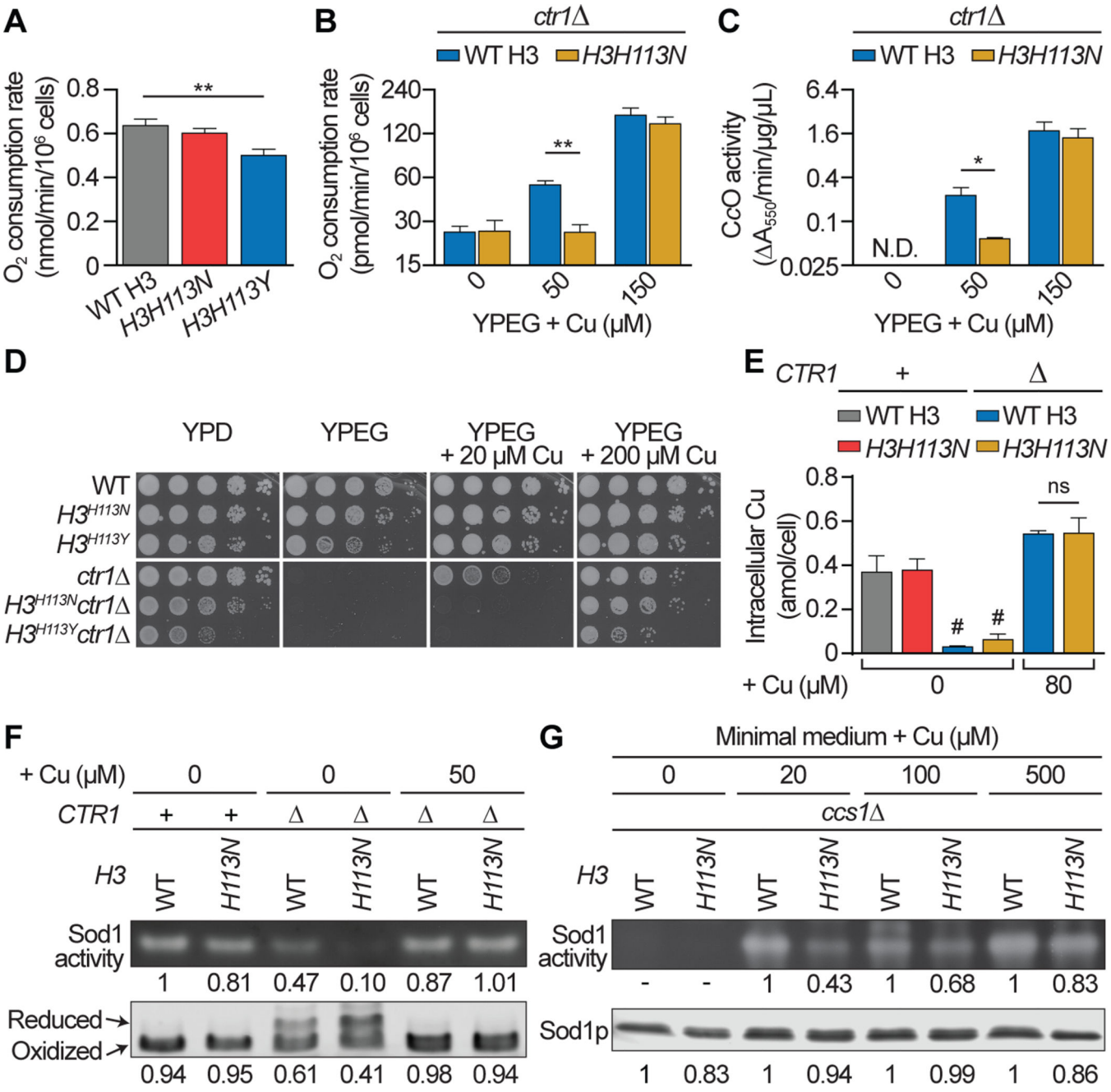

Figure. 5. H3H113 is required for utilization of copper for mitochondrial respiration and Sod1 function.

(A-B) Oxygen consumption assays of cells incubated for 18 hrs **(A)** or 4 hrs **(B)** in liquid YPEG ±$CuSO_4$. Baseline copper concentration in YPEG is ~1 μM. Bars show means in linear **(A)** and log_2 **(B)** scale ±SD from three experiments. Bars in **(A)** are scaled to mitochondrial DNA contents. **(C)** Cytochrome *c* oxidase assays of cells incubated for 4 hrs in liquid YPEG ±$CuSO_4$. Bars show means in log_2 scale ±SD from three experiments. N.D.: not detectable. **(D)** Spot test assays in media ±$CuSO_4$. **(E)** Intracellular copper content of cells grown in YPEG ±$CuSO_4$. Bars show means ±SD from 3–6 experiments. #The *ctr1*Δ

strains, which do not grow in non-fermentable media, were incubated in YPEG for 12 hrs and assessed for metal content for reference. **(F)** Representative Sod1 activity (top) and Sod1 disulfide bond assays (bottom) from three experiments for cells grown in SC ±$CuSO_4$. Relative signal intensities are indicated (bottom numbers are the ratio of oxidized to total Sod1). **(G)** Same as (F), except for cells grown in minimal medium ±$CuSO_4$. Baseline copper concentration in minimal medium is ~0.25 μM. *P≤0.05, **P≤0.01.

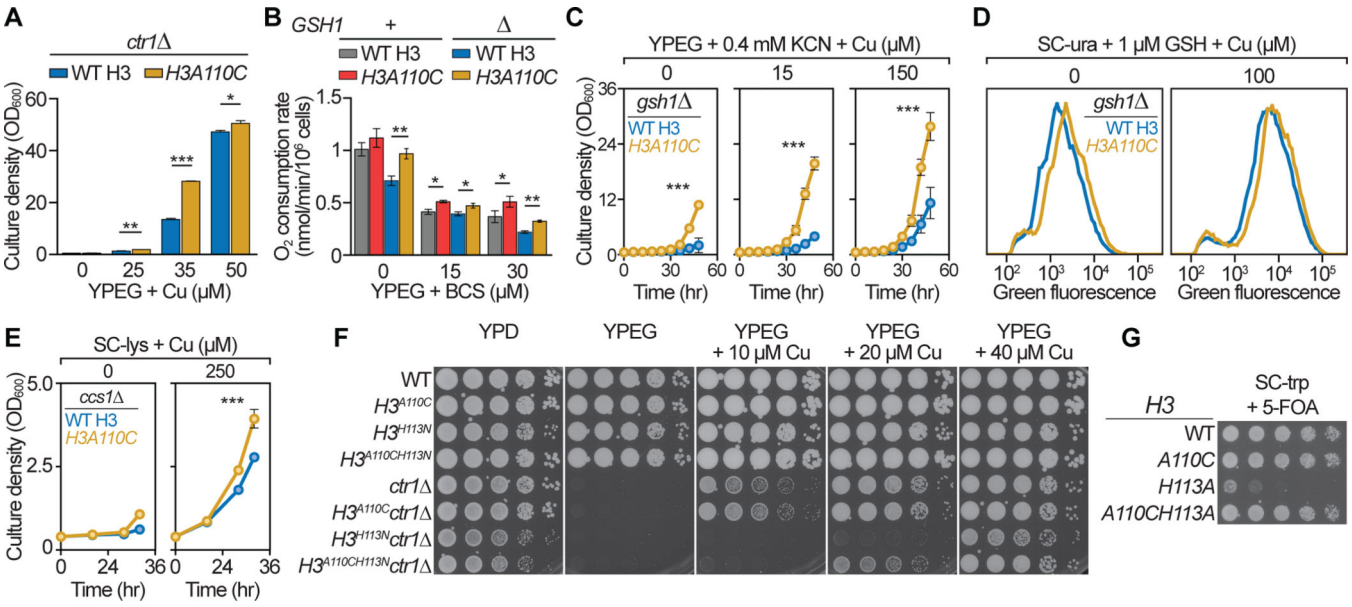

Figure. 6. The *H3A110C* mutation enhances copper utilization in *S. cerevisiae*.

(A) Growth after 48 hrs in liquid YPEG ±$CuSO_4$. Bars show mean OD_{600} ±SD from three experiments. **(B)** Oxygen consumption assays of cells grown in the indicated media for 12 hrs. Bars show mean ±SD of three experiments and are scaled to mitochondrial DNA contents. **(C)** Growth curves in YPEG +potassium cyanide (KCN) ±$CuSO_4$. Lines show means at each time point ±SD from three experiments. P-value is based on all time points. **(D)** Average flow cytometry distributions of cells containing the $p^{(CUP1)}$-GFP plasmid grown in liquid media ±$CuSO_4$ from three experiments. **(E)** Same as (C) but for cells grown in SC-lys ±$CuSO_4$ from four experiments. **(F)** Spot test assays in media ±$CuSO_4$. **(G)** Plasmid shuffle assay with strains harboring WT H3 on a URA3 plasmid and the indicated H3 gene on a TRP1 plasmid. *P<0.05, **P≤0.01, ***P≤0.001.